High-entropy ZrTiCrNiCu coating

To cite this article: V M Yurov *et al* 2021 *J. Phys.: Conf. Ser.* **2064** 012080

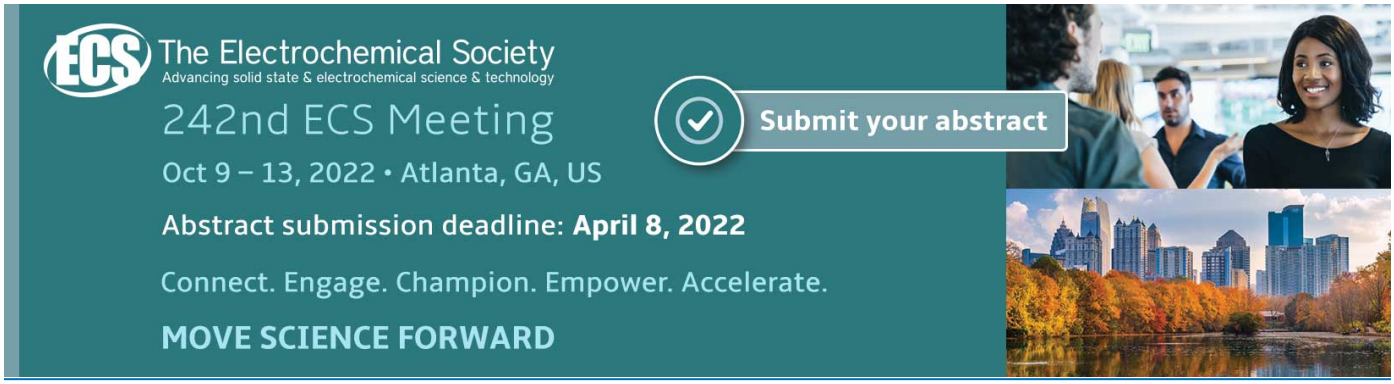

High-entropy ZrTiCrNiCu coating

V M Yurov[1], S A Guchenko[1], V I Goncharenko[2] and V S Oleshko[2]

[1] Karaganda University E A Buketova, 28 Universitetskaya St., Karaganda, 100028, Kazakhstan
[2] Moscow Aviation Institute (National Research University), 4 Volokolamskoe Rd., Moscow, 125993, Russia

E-mail: fvo@mai.ru

Abstract. A magnetron target made of a high-entropy ZrTiCrNiCu alloy was synthesized by mechanical alloying methods followed by annealing in a vacuum furnace. Using this target, coatings were applied to steel samples with a thickness of 7-10 microns. After thermal annealing, the coatings were nanostructured. In terms of microhardness, the ZrTiCrNiCu coating is not inferior to, and in most cases exceeds the hardness of high-entropy equiatomic alloys. A high entropy coating has a low coefficient of friction. They turn out to be anti-friction, which, most likely, leads to energy savings. In this work, the surface energy, contact potential difference and work function of electrons for high-entropy coatings were determined for the first time.

1. Introduction

In high-entropy alloys, as a result of the effect of intense mixing, the entropy contribution increases, which stabilizes the formation of a solid solution with a simple structure [1-3]. Based on Boltzmann's hypothesis on the relationship between entropy and system complexity, the configurational change in entropy ΔS_{conf} during the formation of a solid solution of n elements with equiatomic content can be calculated using the following formula:

$$\Delta S_{\text{conf}} = -R \ln(n^{-1}) = R \ln(n), \quad (1)$$

where R is the universal gas constant, n is the number of mixing elements.

At $n = 5$, $\Delta S_{\text{conf}} = 1.61\,R$ approaches the value of the melting entropy of most intermetallic (about $2R$). However, it was later shown that a high entropy of mixing is not a necessary condition for the formation of a single-phase solid solution, but the very term for the name of such an alloy remains in use.

The mechanisms of friction in nanostructured materials have been poorly studied, possibly due to the difficulty of creating massive samples sufficient for studying friction. In nanostructured materials, the size effect plays a significant role. In [4], nanostructured nickel was obtained by electrodeposition and the coefficient of friction for different grain sizes is shown in figure 1 (a).

Nickel friction coefficient of 0.16 is observed at 8 nm and increases to 0.65 at 61 microns, where the bulk phase already begins. In work [5], the computer method of molecular dynamics (molecular-mechanical theory) was used to check the limits of applicability of the macroscopic description of

contacting nanosurfaces (figure 1 (b)). It turned out that for all types of surfaces the calculated dependences are in excellent agreement with the predictions of the continuum model.

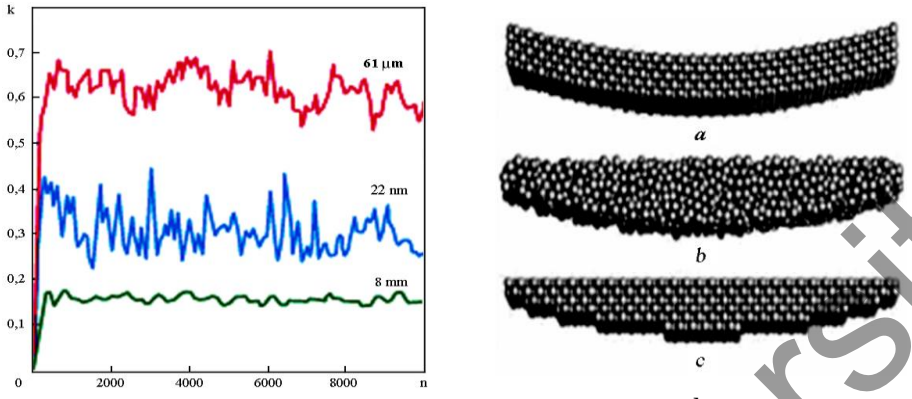

a b

Figure 1. Change in the friction coefficient of nickel with different grain sizes (a) [4], surfaces of the same radius, but with different structures at the atomic level (b) [5].

In this article, we experimentally investigate the friction and microhardness of high-entropy coatings and propose a model that will explain the observed effects within the framework of the energy theory.

2. Experimental technique

High-entropy (HEA) coatings of the composition ZrTiCrNiCu, manufactured by mechanical alloying [6], were used as objects of study. Moreover, after annealing in a vacuum chamber, the samples became nanostructured. In figure 2 (a) shows the studied ZrTiCrNiCu samples; figure 2 (b) their electron microscopic image, and in figure 2 (c) diagram of the formation of nanostructured coatings [7].

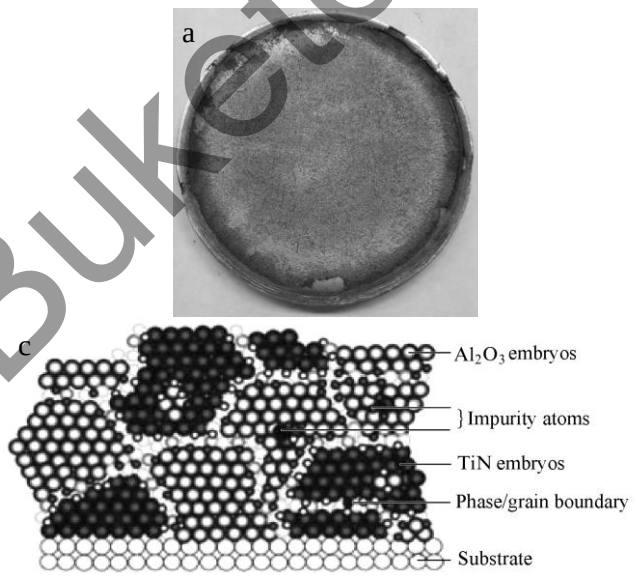

Figure 2. ZrTiCrNiCu sputtering target (a), SEM image of the coating (b) the formation of nanostructured coatings [7].

The roughness of the ZrTiCrNiCu coating, measured with a JSPM-5400 atomic force microscope, is insignificant (figure 3) [8].

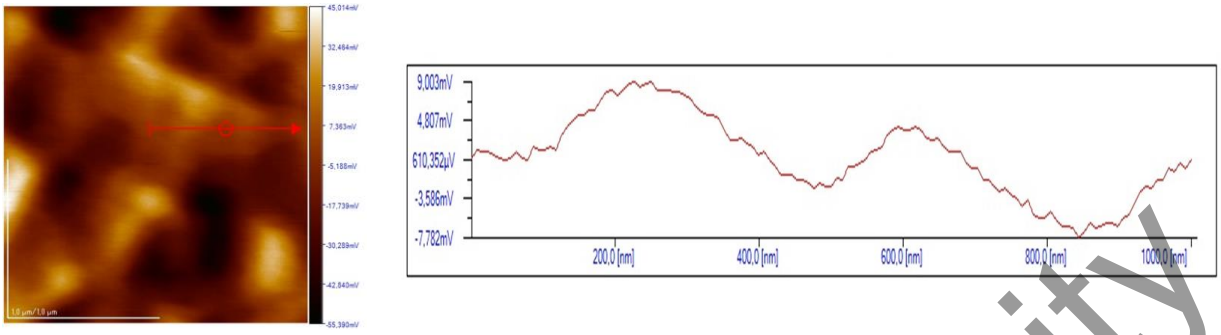

a b

Figure 3. AFM image of ZrTiCrNiCu coating (a) and its roughness (b) [8].

X-ray fluorescence spectroscopy XRF (figure 4) shows that the studied samples is high-entropy coating in the composition from 5 to 35 at.% (table 1).

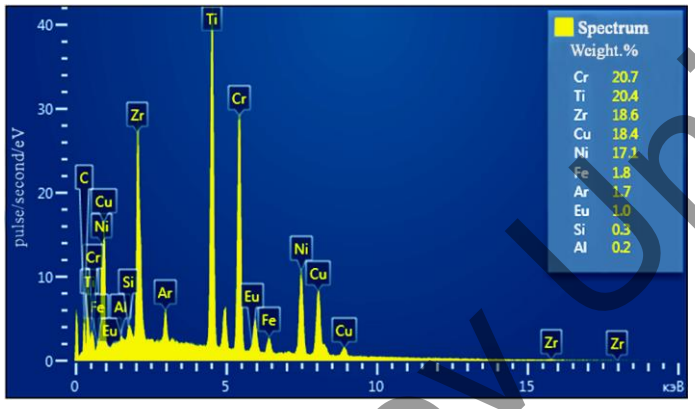

Figure 4. XRF spectrum of ZrTiCrNiCu coating.

Table 1. Quantitative chemical composition of ZrTiCrNiCu (at.%).

Element	Zr	Ti	Cr	Ni	Cu	Impurity
Target	20	20	20	20	20	-
Coating	18.6	20.4	20.7	17.1	18.4	5.0

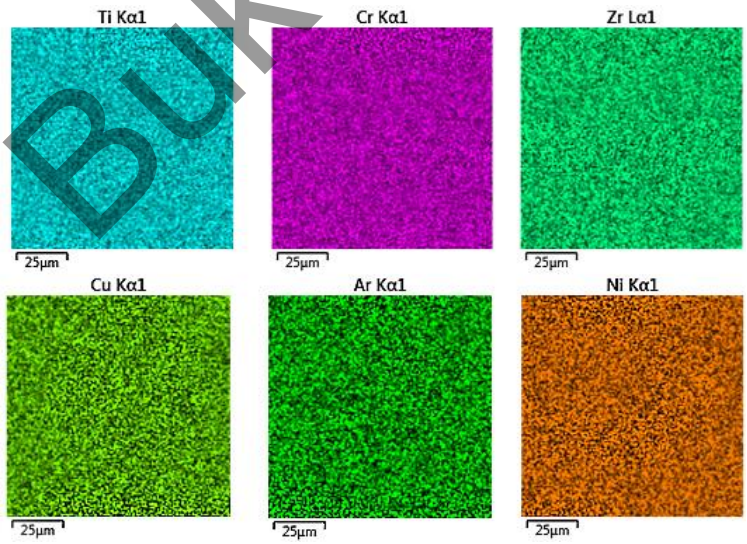

Figure 5. Distribution of ZrTiCrNiCu elements.

Figure 5 shows the distribution of elements in the coverage, which shows that the elements are evenly distributed. This distribution occurs in the coating due to the diffusion process that occurs during thermal annealing of the coating in a vacuum chamber for 3-5 hours.

The phase composition and structural parameters of the samples were studied using an XRD-6000 diffractometer using CuKα radiation.

The phase composition analysis was carried out using PDF 4 + databases, as well as the POWDER CELL 2.4 full-profile analysis program. Table 2 show data on the studied samples.

Table 2. The phase composition of the coating.

Sample	Detected phases	The content of phases (at.%)	Lattice parameters (Å)
ZrTiCrNiCu	$Cu_{1,5}ZrNi_{3.5}$	10	a = 6.7671
	Cu	7.8	a = 3.6178
	$Zr_{0.02}Ni_{0.98}$	19.8	a = 3.5406
	Cr_2Ti	29.5	a = 4.9076 c = 15.9700
	NiTi	33	a = 2.8007 b = 4.6192 c = 4.1824 β = 97.5793

We used a HVS-1000A microhardness tester (figure 6 (a)). This instrument is designed using the latest advances in mechanics, optics, electronics and computer technology to test the hardness of metallic and non-metallic materials, especially small parts or thin hardened layers. The general scheme of the installation for determining the friction coefficients k_{fr} is shown in figure 6 (b) [9] and includes: 1 - known clamping weight, 2 - sample, 3 - sliding surface, 4 - measuring table, 5 - force transducer, 6 - electronics unit and drive.

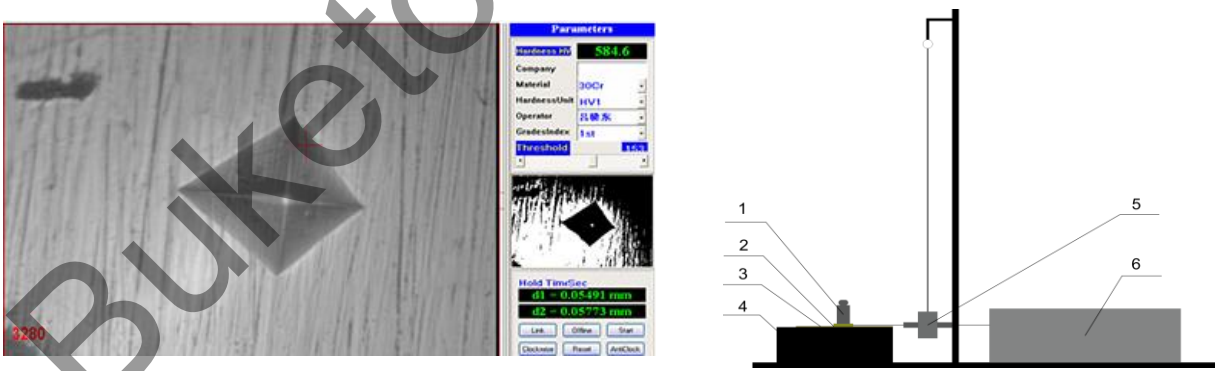

a b

Figure 6. Microhardness tester Hvc-1000A (a) and installation diagram for determining the friction coefficients k_{fr} (b) [9].

Table 3. Microhardness of ZrTiCrNiCu coating (HV0,1 = 0,981 N).

	1	2	3	4	5	6	7	Average
Microhardness HV (MPa)	839	909	864	842	967	753	821	890

The measured microhardness of a coating with a thickness of 7-10 microns with a force of HV 0.1 = 0.981 N is shown in table 3 and, for comparison, in table 4 - the microhardness of other HEAs.

The microhardness of our ZrTiCrNiCu coating is not inferior to highly entropic equiatom alloys.

Table 4. Microhardness of high entropy alloys [10].

Alloys	Initial Hardness cast alloys, HV (MPa)	Alloy hardness after annealing, HV (MPa)
CuTiVFeNiZr	590	600
AlTiVFeNiZr	800	790
MoTiVFeNiZr	740	760
CuTiVFeNiZrCo	630	620
AlTiVFeNiZrCo	790	800
MoTiVFeNiZrCo	790	790
CuTiVFeNiZrCoCr	680	680
AlTiVFeNiZrCoCr	780	
MoTiVFeNiZrCoCr	850	890
316 Stainless steel	189	155
17-4 PH Stainless steel	410	362
Hastelloy C (based Ni-Mo-Fe)	236	280
Stellite 6 (based Co-Cr)	413	494
The microhardness of our ZrTiCrNiCu coating	890	890

The friction coefficients are shown in table 5.

Table 5. Friction coefficients for steel and aluminum.

Coating	for steel		for aluminum	
	coefficient of friction	error	coefficient of friction	error
ZrTiCrNiCu	0.081	0.006	0.066	0.002

High entropy ZrTiCrNiCu coatings turn out to be anti-friction, which in all probability leads to energy savings. The measurement complex of the contact potential difference developed by the authors of [11] is shown in figure 7. The sensor housing was designed in the SolidWorks program and printed on a Picaso 3D Designer 3D printer.

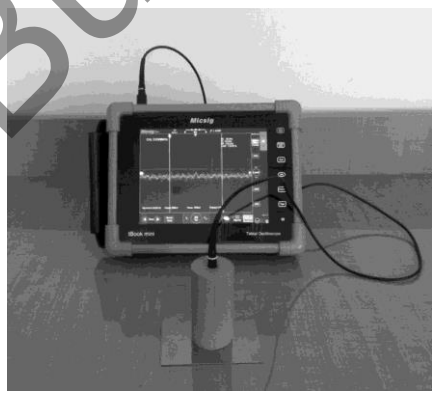

Figure 7. Complex for measuring the contact potential difference of metal parts [11].

The sensor housing is designed to provide a gap between the measuring electrode and the capacitor of 0.5 mm at rest. The advantages of the capacitor method of the contact potential difference are:
- the capacitor can be manufactured with high accuracy;
- the capacitor has low losses (the passage of electric current through capacitive resistance is not accompanied by heat loss) and a high efficiency;
- the shape of the capacitor type sensor can be adapted to various surface shapes of the sample.

The indicated design features of the sensor allow reliable measurements of the contact potential difference of metals (table 6).

Table 6. Surface energy, contact potential difference, and electron work function for the alloy and its composition.

Coating	T_m (K)	σ (J/m^2)	KRP (mV)	φ (eV)
ZrTiCrNiCu	1642	1.149	271	4.73
Ni	1726	1.208	-	4.91-5.01
Cr	2130	1.491	187	4.60
Ti	1943	1.360	-	4.33
Zr	2125	1.488	-	4.12
Cu	1336	0.935	374	4.36

3. Discussion of the experiment results

The table 2 shows the according to A I Rusanov [17] the surface energy is proportional to structural element size r and $\sigma \to 0$ as $r \to 0$ quantitative chemical composition of ZrTiCrNiCu, %, which proves that we have a high-entropy coating. In the table 1 shows the phase composition of the coating. We will discuss this composition.

The first is $Cu_{1.5}ZrNi_{3.5}$ with a phase content of 10 at.% and with a lattice constant equal to a = 6.7671 Å. According to [12, 13], the structure of $Cu_{1.5}ZrNi_{3.5}$ is B2 – a high-temperature austenitic phase ordered by the CsCl type (Pm3m-fcc).

In second place is Cu with a phase content of 7.8 at.% and lattice constant a = 3.6178 Å. The unit cell of copper is fcc.

Third place is $Zr_{0.02}Ni_{0.98}$ with a phase content of 19.8 at.% and lattice constant a = 3.3406 Å. According to X-ray spectral analysis, the main component of the eutectic is the combination of nickel and zirconium. The eutectic component was identified as a ZrNi intermetallic compound with an fcc lattice corresponding to the space group F 43 m (sphalerite type).

Fourth place is Cr_2Ti with a phase content of 29.5 at.% and lattice constant a = 4.9076 Å and c = 15.9700 Å. Near the $TiCr_2$ composition, intermediate phases with the Laves structure are formed [14].

In fifth place is NiTi with a phase content of 33 at.% and the lattice constant a = 2.8007 Å, b = 4.6192 Å, c = 4.1824 Å, β = 97.5793. According to [15], the results of neutron diffraction studies of quenched alloys in the initial austenitic and martensitic states show that the $Ti_{49.5}Ni_{50.5}$ alloy is in the austenitic state at room temperature. The parameter of its crystal lattice B2 (a) and the degree of long-range atomic order (η) turned out to be a = 0.30125 nm; η = 1.00 ± 0.05. In contrast, the $Ti_{50.5}Ni_{49.5}$ alloy at room temperature is in the B19′ martensite state, which unambiguously follows from the interpretation of the neutron diffraction pattern and allows one to determine its parameters: a = 0.2903, b = 0.4112, c = 0.4636 nm, β = 97.25. The NiTi observed by us turns out to be martensite with the B19′ structure.

Thus, five phases are exposed in the ZrTiCrNiCu coating, three have an MCC structure, $TiCr_2$ gives the Laves phase, and NiTi gives martensite with the B19′ structure.

In [16], we obtained the formula for the friction coefficient:

$$k_{fr} = \text{const} \cdot T \cdot (\sigma \cdot S / \tau \cdot G^0) \cdot \Delta t \cdot \bar{n} \,, \qquad (2)$$

where σ is the surface energy, S is the contact area during friction.

Equation (2) describes the friction coefficient k_{fr} proportional to the time of motion during friction Δt, work of friction forces $A = \sigma S$, electron concentration - n, surface energy - σ, contact area - S and is inversely proportional to the relaxation time - τ and Gibbs energy - G^0 of the thermostat.

For high-entropy coatings $G^0 = H–TS+PV \rightarrow S \sim 2R$ (formula 1) and the friction coefficient should decrease. Its decrease is also associated with the formation of nanostructures (figures 1 (a) and 2 (b, c)) and the dependence of the surface energy σ according to A I Rusanov [17] the surface energy is proportional to structural element size r and $\sigma \rightarrow 0$ as $r \rightarrow 0$.

The surface energy σ linearly depends on the hardness of the alloy: $\sigma = \alpha\ \mu$, α = const, and the destruction of the coating should decrease with a decrease in the surface energy (table 6). An equilibrium state is a state with a minimum of free energy. Figure 8 (a) (according to equation 1) shows an increase in the entropy of mixing with an increase in the number of elements for equimolar alloys. It is seen that the entropy of mixing for the phases of the solid solution increases from a small value for conventional alloys to a large value for high-entropy alloys of the composition [1-3].

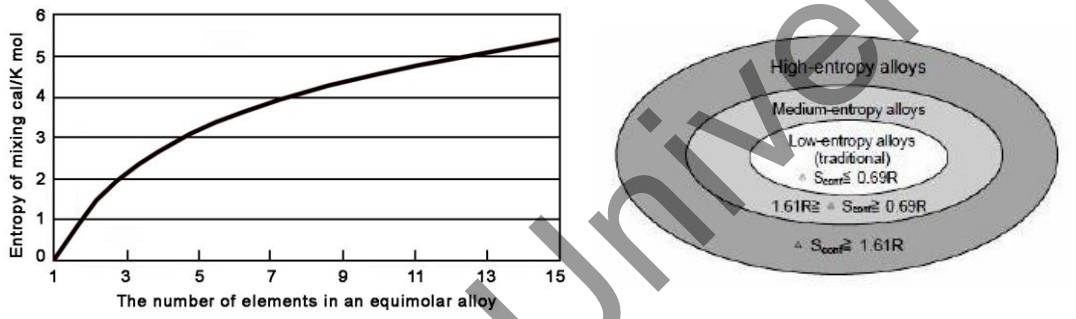

a b

Figure 8. The increase in the entropy of mixing to the number of elements in equimolar alloys in a disordered state (a), the division of the world of alloys by the entropy of mixing (b) [1-3].

Based on the effect of entropy of mixing, it is possible to divide the variety of alloys into three fields, as shown in figure 8 (b). Low entropy alloys are traditional alloys. High-entropy alloys are alloys with at least five basic elements. Medium entropy alloys are alloys with 2...4 basic elements. The high-entropy effect of activation of the formation of a disordered solid phase occurs essentially in the field of high-entropy alloys and should be present to a lesser extent in medium-entropy alloys. Stabilization of a simple solid solution phase is important for the microstructure and properties that can be obtained in these materials [1-3].

This microhardness of the ZrTiCrNiCu coating (table 3) means that the coating structure is not only high-entropy, but also ordered. The ordering of the coating corresponds, as a rule, to dissipative structures. They differ from equilibrium structures in that for their existence they require a constant influx of energy from the outside (magnetron deposition of a coating). It is obvious that dissipative structures can form only in dissipative systems under critical conditions. The transition of a dissipative system to an ordered state is associated with the instability of the previous, disordered one. In this case, a certain parameter of the system exceeds the critical value. With the transition to a new structural state, the system acquires a new way of functioning, ensuring its stability in a new state.

4. Conclusion

Thus, five phases are exposed in the ZrTiCrNiCu coating, three have an MCC structure, $TiCr_2$ gives the Laves phase, and NiTi gives martensite with the B19′ structure.

The proposed high-entropy coating ZrTiCrNiCu on details of enterprises is based on its high hardness (890 MPa) and low friction coefficient (0.04), which leads to an increase in wear resistance

and increases the service life of these parts by 3-4 times. High-entropy coatings due to the small thickness (~ 7-10 microns) of parts of enterprises can be applied again after abrasive wear. High-entropy coatings have unique properties due to the formation of a nanostructure in the surface layer. We have shown this theoretically [16], considering them by the method of quantum thermodynamics of irreversible processes, and experimentally, considering them by the methods of electron microscopy, microhardness tester and automatically measuring the friction coefficients. Equation (2) describes the friction coefficient k proportional to the time of motion during friction Δt, the work of friction forces $A = \sigma s$, surface energy σ, contact area s and is inversely proportional to the relaxation time τ and Gibbs energy G^0 of the thermostat.

For high-entropy coatings $G^0 = H–TS + PV \rightarrow S \sim 2R$ and the friction coefficient should decrease. Its decrease is also associated with the formation of nanostructures and the dependence of the surface energy σ according to A I Rusanov [17] the surface energy is proportional to structural element size r and $\sigma \rightarrow 0$ as $r \rightarrow 0$.

Acknowledgement
The work was carried out under the program of the Ministry of Education and Science of the Republic of Kazakhstan Grants No. 0118RK000063 and No. F.0780.

References
[1] Yeh J-W, Chen S-K, Lin S-J, Gan J-Y, Chin T-S, Shun T-T, Tsau C-H and Chang S-Y 2004 *Adv. Eng. Mater.* **6** 299–303
[2] Yeh J W, Chen Y L, Lin S J and Chen S K 2007 *Mater. Sci. Forum* **560** 1–9
[3] Wang Y P, Li B S and Fu H Z 2009 *Adv. Eng. Mater.* **11** 641–4
[4] Stolyarov V V 2015 *Izvestiya vuzov. Chernaya metallurgiya (Izvestiya. Ferrous Metallurgy)* **58** 597–602 [in Russia]
[5] Luan B and Robbins M O 2005 *Nature* **435** 929–32
[6] Yurov V M, Guchenko S A and Tvardovsky A N 2020 *Trends in the development of science and education* **60** 28–33 [in Russia]
[7] Pogrebnyak A D, Bagdasaryan A A, Pshik A V and Dyadyura K 2017 *Phys.-Usp.* **60** 586–607
[8] Yurov V M, Guchenko S A and Makhanov K M 2020 *International Journal of Applied and Fundamental Research* **4** 62–7 [in Russia]
[9] Yurov V M and Guchenko S A 2020 *School of Science* **1** 5–8 [in Russia]
[10] Kuznetsov A V, Shaysultanov D G, Stepanov N D, Salishchev G A and Senkov O N 2012 *Mater. Sci. Eng.* A **533** 107–18
[11] Yurov V M and Oleshko V S 2019 *Eurasian Physical Technical Journal* **16** 99–108
[12] Firstov G, Koval Y, Timoshevskii A, Yablonovskii S and Humbeeck J V 2013 *Chemistry of Metals and Alloys* **6** 205–8
[13] Kosorukova T, Firstov G, Koval Y, Verhovlyuk P, Humbeeck J V and Noel H 2015 *MATEC Web of Conferences* **33** 06005
[14] Lyakishev N P 1996-2000 *State diagrams of binary metal systems* (Moscow: Mashinostroenie) [in Russia]
[15] Pushin V G, Kuranova N N, Kourov N I, Valiev R Z, Valiev E Z, Makarov V V, Pushin AV and Uksusnikov A N 2012 *Tech. Phys.* **57**(8) 1106
[16] Yurov V M, Zavatskaya O N and Guchenko S A 2012 *Bulletin of the Karaganda university Physics series* **65** 49–56 [in Russia]
[17] Rusanov A I 1967 *Phase Equilibria and Surface Phenomena* (Leningrad: Publishing house Khimia) [in Russia]